Journal of Theoretical and Applied Mechanics, Sofia, Vol.XX (20XX) pp. 1-15
SOLID MECHANICS

TRANSVERSE CRACK AND MASS UNBALANCE INTERACTION IN A SPINNING ROTOR: A THEORETICAL STUDY

NABAM TEYI*, SANDEEP SINGH

Department of Mechanical Engineering, North Eastern Regional Institute of Science and Technology, Nirjuli, Arunachal Pradesh, India – 791109

[Received: 16 June 2023

ABSTRACT: This paper investigates the response of a cracked rotor to varying angles between the crack front and the unbalanced force vector caused by changing centrifugal forces. A rotor with a switching crack is first mathematically represented, and then the response is generated using SIMULINK. At varied angles, the combined effect of crack and imbalance is observed. Maximum and minimum rotor deflection values are depicted on the orbit plots, and their difference with respect to the angles are noted. For various harmonics and vibration amplitudes, a full-spectrum Fast Fourier Transform (FFT) is conducted. Using FFT plots, the critical amplitude of vibrations for each variable angle is determined, and observations are given. This report finishes with some concluding remarks.

KEY WORDS: Full spectrum Fast Fourier Transform, Mass unbalance, Orbit plots, Rotor cracks, Switching cracks.

NOTATIONS

x, y	Inertial coordinates
i	Harmonic number
j	Complex number, $\sqrt{-1}$
β	Angle made by crack front and mass unbalance axes
η	Rotating coordinate along crack front
ψ	Rotating coordinate normal to crack front
ω	Spin speed, rad/s
m	Mass, kg
c	Viscous damping, Ns/m
t	Time, s
v_x	Displacement in x direction
v_y	Displacement in y direction
v_η	Displacement in η direction
v_ψ	Displacement in ψ direction
p_0	Intact shaft flexibility
Δp_η	Additive crack flexibility
p_ψ	Cross flexibility
f_η	Excitation force in η direction
f_ψ	Excitation force in ψ direction
q_0	Intact shaft stiffness
Δq_η	Stiffness lost due to crack
$s(t)$	Crack force steering function
rot	Rotating
st	Static
unb	Unbalance
cr	Crack

*Corresponding author e-mail: nbt@nerist.ac.in

VECTORS AND MATRICES

$\mathbf{f}$	Force	$\mathbf{h}$	Total displacement
$\mathbf{T}$	Transformation matrix	$\mathbf{Q}$	Stiffness
$\mathbf{Q}_0$	Intact shaft stiffness	$\Delta\mathbf{Q}$	Additive stiffness due to crack
$\mathbf{H}$	Total displacement	$\mathbf{h}_0$	Static displacement
$\Delta\mathbf{h}$	Vibration displacement	$\mathbf{M}$	Stiffness lost due to crack

1 INTRODUCTION

A rotor is a shaft with a disc on it that is supported by bearings. The function of a rotor is to receive motion from one unit and then transmit it to other units. Rotors are primarily motion transmission mechanisms that are used in practically all mechanical machineries. A faulty rotor is a very common cause of machinery failure. There is a detailed survey of literatures on rotor cracks of the recent decade [1]. Although fresh rotors are subjected to non-destructive tests and other quality checks before being installed in a machine, the existence or absence of faults is determined in real time while the machine is in operation, by continuous signal monitoring based on data science tool [2].

Mass unbalance is another imperative component that causes deviation from optimal rotor performance. This mass imbalance causes the physical rotor's axis to drift away from its geometric axis due to the continual centrifugal impact of its spin. Mass unbalance is more natural for a shaft rotor system than emergence of cracks, owing to various inconsistencies and complexities in the manufacturing or extraction of the materials; accumulation of dust or other substances on some locations on its surface; chemical reactions on its surface due to environmental situations; or friction wear. In rotors, the presence of cracks and mass unbalance is a fatal combination.

Several literatures exist on the effect of mass unbalance and crack characteristics on rotor system behavior. In exploring cracked rotor imbalance in nonlinear dynamics, 3D finite element models have been utilized to discretize the rotor and mimic intermittent breathing on cracked surfaces [3]. High unbalance eccentricity and the 180^0 location of the unbalanced mass caused the disappearance of 2X and/or 3X harmonic components at 1/2 and 1/3 of the rotor critical speed [4]. The direction of the unbalance changed the shape of the resonance curve considerably, and when the unbalance was in the same direction as the crack, it created an unstable region [5]. Breathing crack model predicted a stronger response for most imbalance orientation angles than the switching crack model [6]. Vibrational behavior of a harmonic resonance and a 1/2-order sub-harmonic resonance significantly changed due to imbalance angular position changes in a cracked rotor in a nonlinear rotor system as compared to a rotor system with linear supports [7]. Vertical and horizontal responses of the disc and bearings, orbital evolution around nontrivial equilibrium, and Bode

graphs generated by frequency sweep showed that orbital development around 1/2 and 1/3 of the initial resonance could detect rotor cracks even if the crack-imbalance orientation was unknown [8]. Based on the Stress Intensity Factor (SIF), it was noted that the crack always opened when the eccentric mass and crack were in similar positions. The crack wouldn't open if the eccentric mass was opposite it. [9, 10]. The critical speed of a cracked rotor was between the natural frequencies of a fully open and closed crack and dependent on an unbalanced orientation angle. Its value was lowest at 90^0 and highest at 270^0 [11]. Parametric stability of the breathing cracked rotor with unbalanced orientation angles and accelerations showed that instability regimes at fractions or multiples of critical speeds differed with unbalanced orientation angles [12].

Phases of crack unbalance had a substantial effect on the switching crack model's bifurcation features. Depending on the unbalance orientation, the response was chaotic, quasi-periodic, sub-harmonic, or period one [13]. On considering rolling, pitching, and yawing to be sinusoidal disturbances on constant terms; the impacts of base angular motions, frequency and amplitude of base excitations, and crack depths have been discussed [14]. A model-based technique that accurately determined imbalance position, extent, and orientation on real rotor systems was developed [15].

The rotor system's behavior is significantly affected by the combination of the occurrence of a crack and the unavoidable presence of mass unbalance, as evidenced by the literatures cited above. Hence, this paper investigates the influence of relative angles between the transverse crack front and the direction of mass unbalance on the dynamic deflection of the shaft axis from its ideal geometric axis in the x and y dimensions. In addition, the variation in vibration amplitude at significant frequencies is investigated for various relative angles between the transverse crack front and the direction of mass unbalance.

2 Equations of Motion

The rotor keeps the disc close to a transverse crack in the middle of its length as shown in Fig. 1. A massless shaft is assumed because of the lumped parameter nature of the model. The disc's vertical and horizontal degrees of freedom of translation are both considered. The effects of elastic coupling and gyroscopic are not taken into account.

The crack creates local shaft flexibility, which alters the system's inherent frequency. The opening and closing of the crack are determined by its instantaneous position with regard to the deflected shaft's neutral axis [16]. When in the tensile zone, the crack remains open; when in the compression zone, it closes. If the crack only has two possible states, fully closed and fully open, with no intermediate state, then the transition from open to closed and closed to open must be abrupt rather than gradual. Switching cracks are another term for this type of crack.

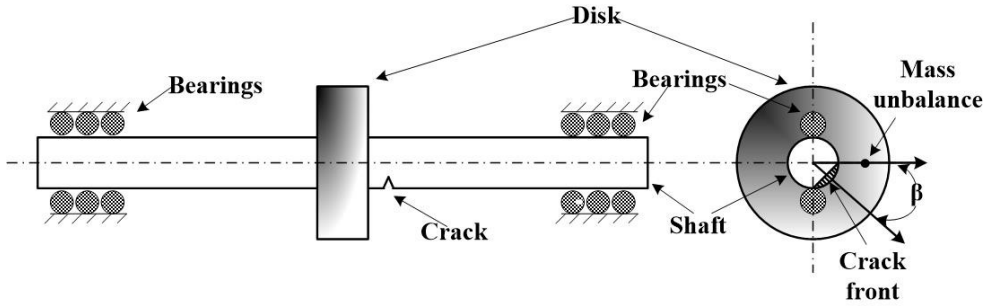

Fig. 1: Rotor system.

As shown in Fig. 2 (a) and (b), the angle between the axis of mass unbalance and the axis of the crack front is denoted by angle β. η is along the crack front axis, ψ is normal to it, and ωt is the angle between x-axis and crack front axis.

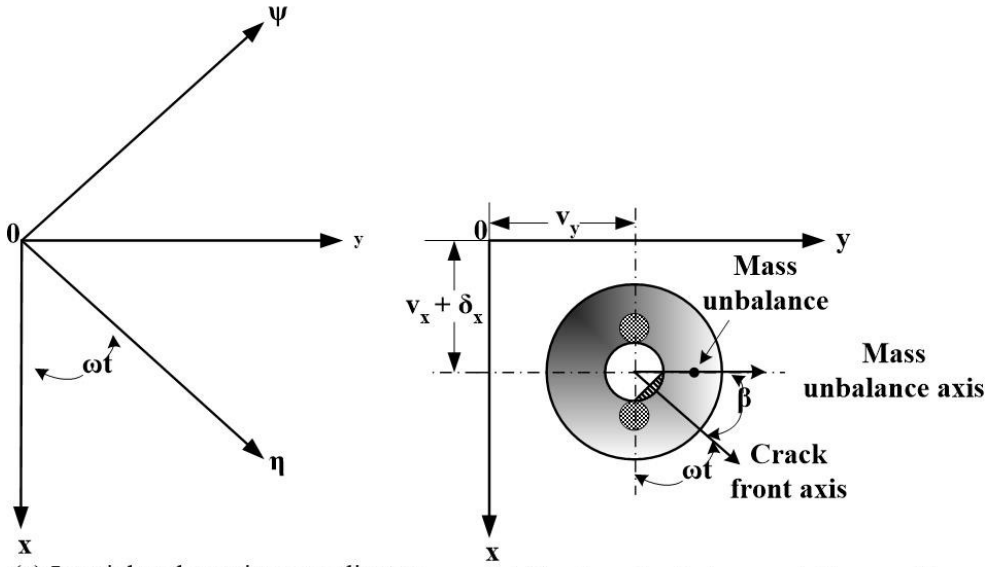

(a) Inertial and rotating coordinates (b) Crack and unbalance relative position

Fig. 2: Coordinate system.

In the rotating coordinate system $\eta - \psi$, the deflection at the point of the disc with an open crack adjacent to it, is

$$\begin{Bmatrix} v_\eta \\ v_\psi \end{Bmatrix}_{rot} = \begin{bmatrix} p_0 + \Delta p_\eta & 0 \\ 0 & p_0 + 0 \end{bmatrix} \begin{Bmatrix} f_\eta \\ f_\psi \end{Bmatrix}_{rot}, \tag{1}$$

where p_0 is the round undamaged shaft's flexibility, and Δp_η is the increased flexibility owing to the crack. In the coordinate axis directions η and ψ, f_η and f_ψ are excitation forces. The cross-flexibility Δp_ψ introduced by the existence of a crack is several times smaller than the primary flexibility Δp_η, except in the case of slow roll or very deep cracks. And therefore Δp_ψ has been removed from the equation. As the shaft rotates, the crack will close as it hits the compressive zone, and Δp_η will become zero. The shaft now acts as though the crack does not exist. Equation (1)'s flexibility matrix can be decomposed into two matrices containing p_0 and Δp_η, because p_0 is constant and Δp_η has a periodicity of 2π

$$\begin{Bmatrix} v_\eta \\ v_\psi \end{Bmatrix}_{rot} = \left(\begin{bmatrix} p_0 & 0 \\ 0 & p_0 \end{bmatrix} + \begin{bmatrix} \Delta p_\eta & 0 \\ 0 & 0 \end{bmatrix} \right) \begin{Bmatrix} f_\eta \\ f_\psi \end{Bmatrix}_{rot} . \tag{2}$$

In the rotating coordinate system, the restoring force vector can be produced by inverting the flexibility matrix and adding the steering function, $s(t)$, to account for the periodicity of Δq_η:

$$\begin{Bmatrix} f_\eta \\ f_\psi \end{Bmatrix}_{rot} = \left(\begin{bmatrix} q_0 & 0 \\ 0 & q_0 \end{bmatrix} - s(t) \begin{bmatrix} \Delta q_\eta & 0 \\ 0 & 0 \end{bmatrix} \right) \begin{Bmatrix} v_\eta \\ v_\psi \end{Bmatrix}_{rot} \tag{3}$$

with $(1/p_0) = q_0$ and $1/(p_0 + \Delta p_\eta) = q_0 - \Delta q_\eta$.

The stiffness of the undamaged shaft is q_0, while the stiffness loss owing to the crack opening is Δq_η. The steering function $s(t)$ is 0, for the compressive zone crack, and $s(t)$ is 1, for the tensile zone crack. A transformation can be used to derive the restoring force vector in inertial coordinates as:

$$\mathbf{f}(t)_{sp} = \mathbf{Q}(t)\mathbf{h}(t) \tag{4}$$

with

$$\mathbf{f}(t)_{sp} = \begin{Bmatrix} f_x(t) \\ f_y(t) \end{Bmatrix} = \mathbf{T} \begin{Bmatrix} f_\eta(t) \\ f_\psi(t) \end{Bmatrix} ,$$

$$\mathbf{T}(t) = \begin{bmatrix} \cos\omega t & \sin\omega t \\ -\sin\omega t & \cos\omega t \end{bmatrix} ,$$

$$\mathbf{Q}(t) = \mathbf{Q}_0 + \Delta\mathbf{Q}(t) = \mathbf{T}^{-1}(\mathbf{Q}_{0,rot} + \Delta\mathbf{Q}(t)_{rot})\mathbf{T} ,$$

$$\mathbf{Q}_0 = \begin{bmatrix} q_0 & 0 \\ 0 & q_0 \end{bmatrix} ,$$

$$\Delta\mathbf{Q}(t) = -\frac{1}{2} s(t) \Delta q_\eta \begin{bmatrix} 1 + \cos 2\omega t & \sin 2\omega t \\ \sin 2\omega t & 1 - \cos 2\omega t \end{bmatrix}$$

$$\text{and} \quad \mathbf{h}(t) = \Delta\mathbf{h}(t) + \mathbf{h}_0 = \begin{Bmatrix} v_x(t) \\ v_y(t) \end{Bmatrix} + \begin{Bmatrix} \delta_x \\ 0 \end{Bmatrix} = \mathbf{T} \begin{Bmatrix} v_\eta(t) \\ v_\psi(t) \end{Bmatrix} + \mathbf{T} \begin{Bmatrix} (\delta_{st})_\eta \\ (\delta_{st})_\psi \end{Bmatrix} .$$

The inertial frame motion equation for the system has been developed [17]. The equation is expressed in terms of static deflection (δ_x) and vertical and horizontal vibration displacements as (v_x and v_y respectively) as:

$$\mathbf{M}\ddot{\mathbf{h}}(t) + \mathbf{C}\dot{\mathbf{h}}(t) + \mathbf{Q}(t)\mathbf{h}(t) = \mathbf{f}_{st} + \mathbf{f}_{unb}(t) \tag{5}$$

with

$$\mathbf{M} = \begin{bmatrix} m & 0 \\ 0 & m \end{bmatrix}, \qquad \mathbf{C} = \begin{bmatrix} c & 0 \\ 0 & c \end{bmatrix}, \qquad \mathbf{f}_{st} = \begin{Bmatrix} mg \\ 0 \end{Bmatrix},$$

$$\mathbf{f}_{unb}(t) = me\omega^2 \begin{Bmatrix} \cos(\omega t + \beta) \\ \sin(\omega t + \beta) \end{Bmatrix} .$$

Since, $\mathbf{h}(t) = \mathbf{h}_0 + \Delta\mathbf{h}(t)$, therefore, $\ddot{\mathbf{h}}(t) = \Delta\ddot{\mathbf{h}}(t)$ and $\dot{\mathbf{h}}(t) = \Delta\dot{\mathbf{h}}(t)$.

Thus, equation (5) becomes:

$$\mathbf{M}\Delta\ddot{\mathbf{h}}(t) + \mathbf{C}\Delta\dot{\mathbf{h}}(t) + \mathbf{Q}_0\mathbf{h}_0 + \mathbf{Q}_0\Delta\mathbf{h}(t) + \Delta\mathbf{Q}(t)\mathbf{h}_0 + \Delta\mathbf{Q}(t)\Delta\mathbf{h}(t) = \mathbf{f}_{st} + \mathbf{f}_{unb}(t) . \tag{6}$$

Since static deflection (δ_x) in a heavy rotor is relatively great in comparison to vibration-induced displacements, $\Delta\mathbf{Q}\Delta\mathbf{h}$ is very little and consequently overlooked, and $\mathbf{Q}_0\mathbf{h}_0$ equals to $\mathbf{f}_{st}$. Hence, equation (6) becomes:

$$\mathbf{M}\Delta\ddot{\mathbf{h}}(t) + \mathbf{C}\Delta\dot{\mathbf{h}}(t) + \mathbf{Q}_0\Delta\mathbf{h}(t) = \mathbf{f}_{st} + \mathbf{f}_{unb}(t) \tag{7}$$

with $\mathbf{f}_{cr}(t) = -\Delta\mathbf{Q}(t)\mathbf{h}_0$.

Equation (7) has all of the information about the cracked rotor (crack and unbalance). On the left side of the equation, mass, damping, and stiffness of the whole shaft are given. On the right, force due to time-varying crack stiffness, $\mathbf{f}_{cr}$, and imbalance are given.

3 Generation of Response

Considered here is a method for approximating a switching crack with a rectangular waveform [18]. Switching crack excitation function (SCEF), or the steering function $s(t)$, is written as:

$$s(t) = \frac{1}{2} + \frac{2}{\pi}\cos\omega t - \frac{2}{3\pi}\cos(3\omega t) + \frac{2}{5\pi}\cos(5\omega t) - \frac{2}{7\pi}\cos(7\omega t) + \frac{2}{9\pi}\cos(9\omega t). \tag{8}$$

Equation (7) is used to create a SIMULINK™ model that is used to simulate displacement and current responses as shown in Fig. 3. The SCEF, written as $s(t)$, is

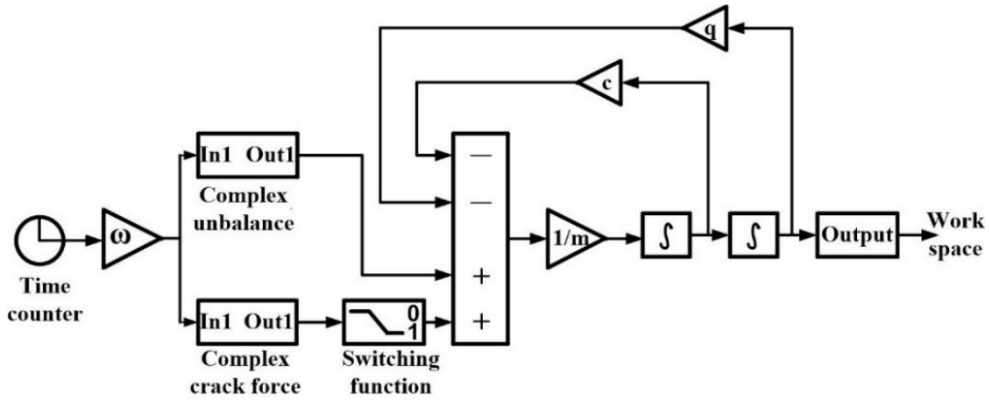

Fig. 3: Simulink model.

based on equation (8). The model now has a way to make the quadrature reference signal with the form $\cos(i\omega t) + j\sin(i\omega t)$, where i can only be one of the harmonics of interest. The phase correction of the quadrature signal used in identification can be helped by making and using this kind of quadrature reference signal.

Clock is the time counter; triangular blocks perform multiplication operation. The summing block, represented by the rectangular blocks and arranged in accordance with equation (7) does the algebraic operations on the input signals, carried out by the summation blocks in the order that the $+$ and $-$ signs appear inside the block. The force term is the sum total of the summation block. The $\int$ block numerically integrates the input signal. The acceleration term is obtained by multiplying by $1/m$ before the integration block. The integration blocks with this input provide velocity and displacement in both orthogonal directions. Switching function for crack force is developed by implementing a $0-1$ switch. Operating parameters such as the spin speed (ω), mass (m) and viscous damping (c) are placed in their respective blocks. The constants block contains the unbalance phase β.

4 Result and Discussion

With the rotor crack modeling done and response generated in the preceding section, here we first observe the deviation and behavior of deflection of the spinning shaft from its ideal central axis in x and y directions through orbit plots. The observation is made starting with the both the axes of crack front and mass unbalance being in line in the same direction, i.e., $\beta = 0°$. Then this angle between the mass unbalance and the crack is incremented for 15° for each observation till β reaches 360°. And secondly, the amplitude of vibration is recorded for various frequencies for each step β increment using Fast Fourier Transform (FFT) plots.

4.1 ORBIT PLOTS

The orbit plots are obtained for each 15° increments from $\beta = 0°$ to $\beta = 360°$. These plots represent the x and y deviation from the mean axis. A few of such plots for different β are shown in Fig. 4. The horizontal axis notes the x values while the vertical axis shows the y values.

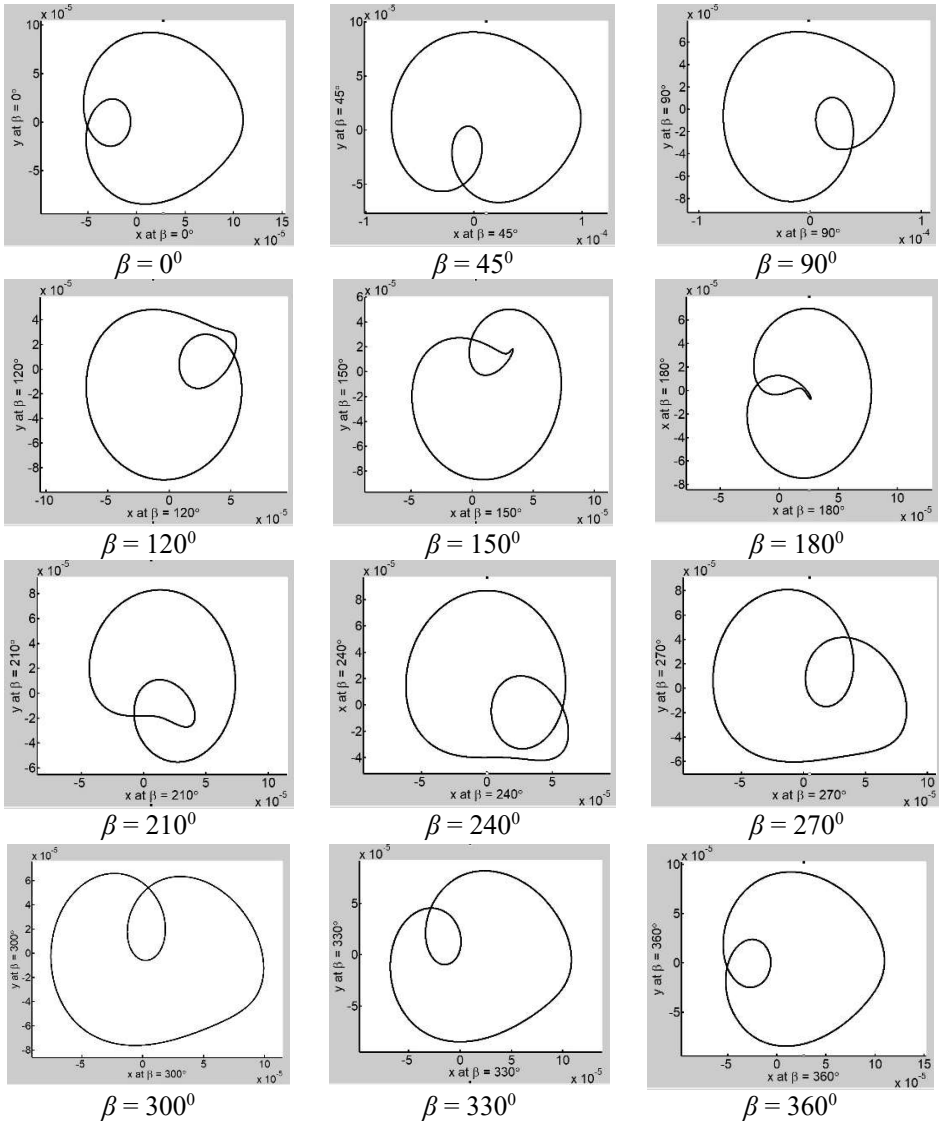

Fig. 4: Orbit plots.

It is observed from the orbit plots that variations exist in the way the shaft deflects in orthogonal directions as the angle between the crack front and the mass unbalance varies. The minimum and maximum values of x and y have been picked/ticked and noted. Table 1 shows the values of minimum deviation in x direction as $x_{\min}$, maximum deviation in x direction as $x_{\max}$ and their difference as x_{length}, as well as of minimum deviation in y direction as $y_{\min}$, and maximum deviation in y direction as $y_{\max}$ and their difference as y_{length}, with respect to β from 0° to 360°.

Figure 5 (a) shows the graph of x_{length} (difference between the maximum and minimum deviation of the shaft from its ideal geometric axis in x direction) with respect to β (various relative angular positions of crack front with respect to mass unbalance). While Fig. 5 (b) shows the variation of y_{length} for different β.

Table 1: Variations of x and y displacements for different relative angle between crack and unbalance

β	$x_{\min}$ [10^{-5} m]	$x_{\max}$ [10^{-5} m]	x_{length} [10^{-5} m]	$y_{\min}$ [10^{-5} m]	$y_{\max}$ [10^{-5} m]	y_{length} [10^{-5} m]
0°	-5.492	10.96	16.452	-8.428	9.246	17.674
15°	-6.396	10.76	17.156	-8.06	9.418	17.478
30°	-7.133	10.4	17.533	-7.473	9.369	16.842
45°	-7.661	9.897	17.558	-6.691	9.073	15.764
60°	-7.958	9.25	17.208	-6.686	8.55	15.236
75°	-8.016	8.458	16.474	-7.55	7.813	15.363
90°	-7.82	7.558	15.378	-8.254	6.938	15.192
105°	-7.377	6.477	13.854	-8.734	5.92	14.654
120°	-6.724	5.879	12.603	-8.97	4.844	13.814
135°	-5.891	6.676	12.567	-8.952	3.912	12.864
150°	-4.921	7.278	12.199	-8.679	5.023	13.702
165°	-3.848	7.658	11.506	-8.17	6.055	14.225
180°	-2.746	7.786	10.532	-7.445	6.992	14.437
195°	-3.291	7.687	10.978	-6.543	7.754	14.297
210°	-4.337	7.343	11.68	-5.514	8.31	13.824
225°	-5.351	6.77	12.121	-4.419	8.625	13.044
240°	-6.21	6.232	12.442	-4.211	8.703	12.914
255°	-6.867	7.319	14.186	-5.028	8.506	13.534
270°	-7.338	8.326	15.664	-6.019	8.083	14.102
285°	-7.552	9.207	16.759	-6.896	7.451	14.347
300°	-7.533	9.931	17.464	-7.61	6.588	14.198
315°	-7.278	10.48	17.758	-8.142	7.319	15.461
330°	-6.787	10.83	17.617	-8.463	8.157	16.62
345°	-6.108	10.99	17.098	-8.563	8.809	17.372
360°	-5.491	10.96	16.451	-8.419	9.226	17.645

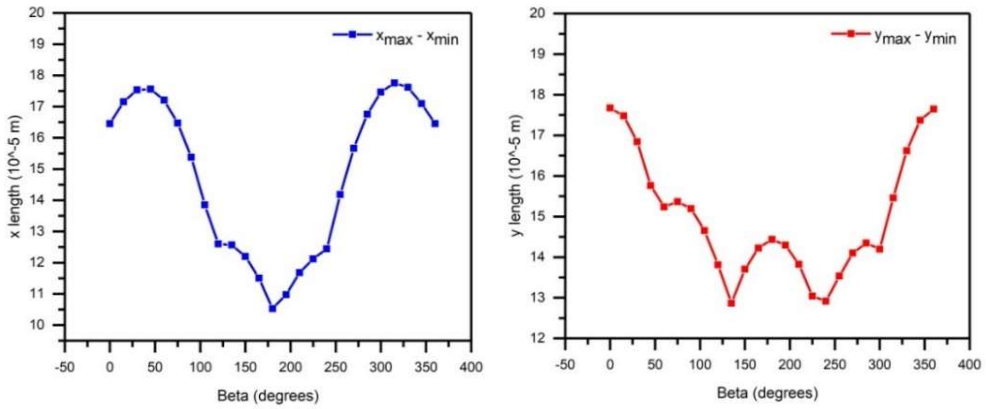

(a) x deviation vs β (b) y deviation vs β

Fig. 5: Variations of x and y displacements for different β.

In the above graphs, β has been denoted as Beta in degrees while the deflections have been marked at 10^-5 meters. The graphs above indicate that near symmetry exist for both the x and y axes around 180°. The graphs should have had perfect symmetry, however owing to errors in picking/ticking maximum and lowest x and y values from the orbit plots, they only have near perfect symmetry. The symmetry is due to the fact that the effect of the crack front's angular position with regard to unbalance is the same whether it is positioned on the positive or negative side of the unbalance axis. As an example, β as 30° has the same effect on shaft behavior as β as 330° (i.e. -30°). Furthermore, for the least x deflection is found at $\beta = 180°$, indicating that when the crack axis sits exactly opposite the unbalance axis, the crack opening is minimal, implying that the unbalance tends to nullify the influence of the crack on the shaft. The x deflection is found to increase from $\beta = 0°$ to its maximum around $\beta = 45°$, and then it decreases thereon to its minimum at $\beta = 180°$. It means that the imbalance aggravates the detrimental effect on the rotor system when the crack axis is in alignment with its direction and is the worst when it is 45°.

The lowest y deflection values are observed at $\beta = 135°$ and near symmetrically at 225°. The maximum y values are observed when the crack and the unbalance are in line in the same direction i.e., at $\beta = 0° = 360°$. This means that the shaft is at its weakest when both forces are acting in the same direction.

4.2 Fast Fourier Transform (FFT) plots

Full spectrum FFT can manage phase ambiguity [19]. Here, full spectrum FFT for various β are performed, a few of which are shown in Fig. 6 below.

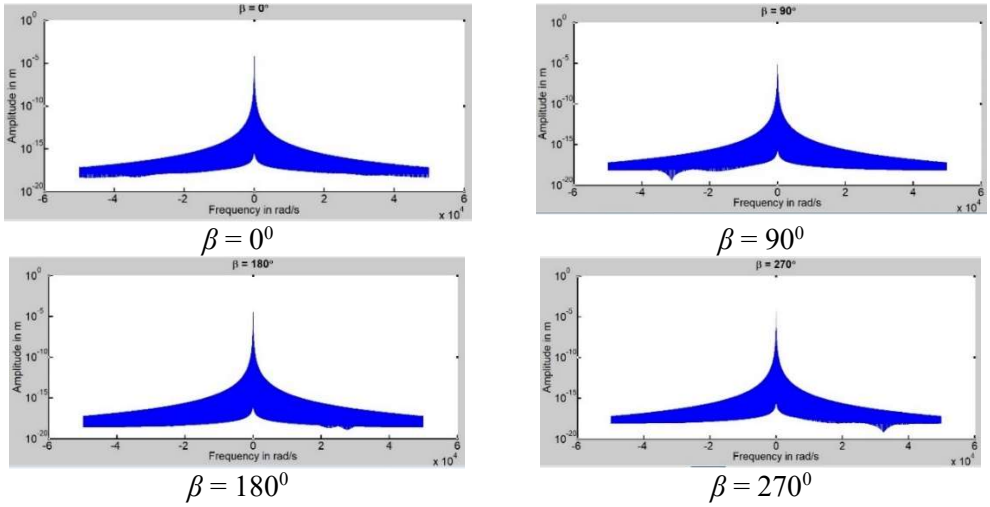

$\beta = 0^0$ $\beta = 90^0$ $\beta = 180^0$ $\beta = 270^0$

Fig. 6: FFT plots.

In the above plots, the abscissa marks the frequency in radian per second, while the ordinate shows the vibration amplitude in meters. Amplitudes are uniform at high frequencies (both negative and positive) for all β. And since, substantial amplitudes are only observed around the direct current, i.e., at 0^{th} harmonics, the entire FFTs are

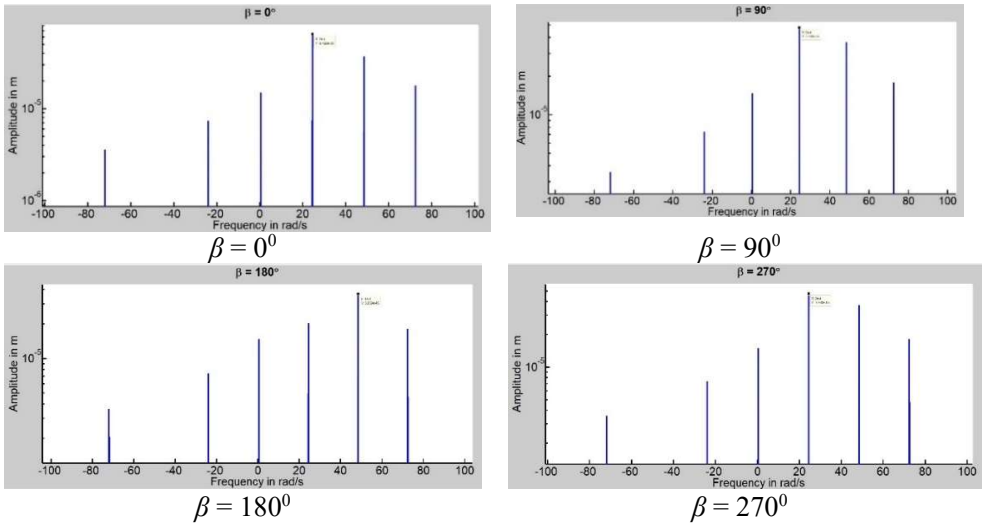

$\beta = 0^0$ $\beta = 90^0$ $\beta = 180^0$ $\beta = 270^0$

Fig. 7: Frequency vs amplitude.

exploded around 0^{th} harmonics for close examination. A few of such zoomed FFTs are shown in Fig. 7. Here amplitudes are noted only for -3x, -2x, -1x, 0, 1x, 2x, and 3x harmonics.

The highest value of amplitude for each β has been picked/ticked at the particular harmonics and noted. Table 2 lists the values of amplitudes for -3x, -2x, -1x, 0, 1x, 2x, and 3x frequencies for different β.

Table 2 shows that there is no amplitude of vibration at -2x frequency, i.e., -2ω harmonics equals 0. In fact, 4x or 4ω harmonics is also equal to 0. This is due to the fact that every square wave, when expanded in Fourier series forms, has no -2x, 4x harmonics. This is a mathematical principle. And, because this paper is not

Table 2: Amplitudes at for -3x, -2x, -1x, 0, 1x, 2x, and 3x frequencies for different β

β	-3x [10^{-5} m]	-2x [10^{-5} m]	-1x [10^{-5} m]	0 [10^{-5} m]	1x [10^{-5} m]	2x [10^{-5} m]	3x [10^{-5} m]
0°	0.3581	0	0.7354	1.474	6.428	3.659	1.79
15°	0.3581	0	0.7354	1.474	6.378	3.659	1.79
30°	0.3581	0	0.7354	1.474	6.23	3.659	1.79
45°	0.3581	0	0.7354	1.474	5.988	3.659	1.79
60°	0.3581	0	0.7354	1.474	5.657	3.659	1.79
75°	0.3581	0	0.7354	1.474	5.245	3.659	1.79
90°	0.3581	0	0.7354	1.474	4.763	3.659	1.79
105°	0.3581	0	0.7354	1.474	4.227	3.659	1.79
120°	0.3581	0	0.7354	1.474	3.657	3.659	1.79
135°	0.3581	0	0.7354	1.474	3.085	3.659	1.79
150°	0.3581	0	0.7354	1.474	2.561	3.659	1.79
165°	0.3581	0	0.7354	1.474	2.167	3.659	1.79
180°	0.3581	0	0.7354	1.474	2.015	3.659	1.79
195°	0.3581	0	0.7354	1.474	2.167	3.659	1.79
210°	0.3581	0	0.7354	1.474	2.561	3.659	1.79
225°	0.3581	0	0.7354	1.474	3.085	3.659	1.79
240°	0.3581	0	0.7354	1.474	3.657	3.659	1.79
255°	0.3581	0	0.7354	1.474	4.227	3.659	1.79
270°	0.3581	0	0.7354	1.474	4.763	3.659	1.79
285°	0.3581	0	0.7354	1.474	5.245	3.659	1.79
300°	0.3581	0	0.7354	1.474	5.657	3.659	1.79
315°	0.3581	0	0.7354	1.474	5.988	3.659	1.79
330°	0.3581	0	0.7354	1.474	6.23	3.659	1.79
345°	0.3581	0	0.7354	1.474	6.378	3.659	1.79
360°	0.3581	0	0.7354	1.474	6.428	3.659	1.79

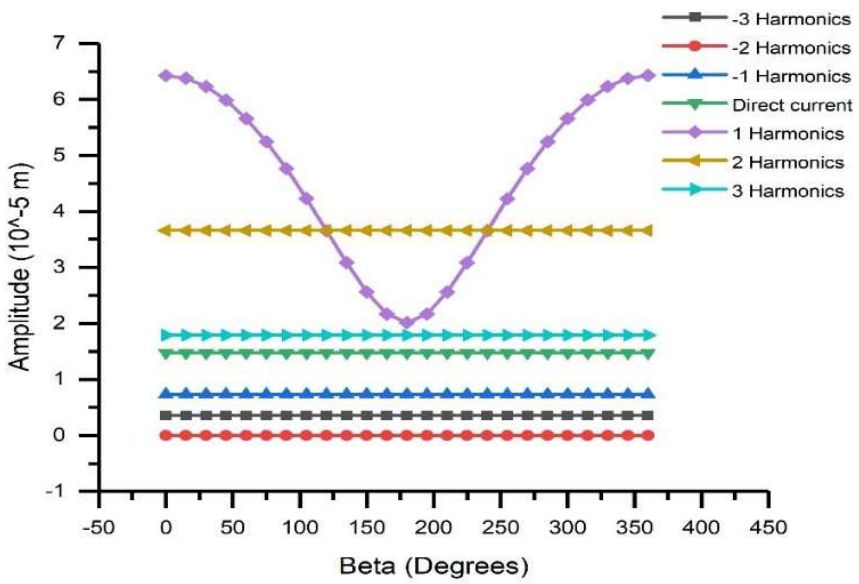

Fig. 8: Amplitude vs β for various harmonics.

about gaping cracks, where the crack gradually opens and closes, but about switching cracks, where the crack is either fully open or fully closed, the crack behavior for one shaft spin will be a square wave, with the square wave bottom line representing a closed crack and the top line representing a fully open crack. For each spin, the crack opens in the tensile zone and closes in the compressive zone. In fact, the absence of -2ω, 4ω and other harmonic terms is confirmed by equation (8), which represents the switching crack excitation function. The values of the above table is represnted in a graph plot in Fig. 8.

In the above graph, β has been denoted as Beta in degrees while the amplitudes of vibration have been marked at 10^-5 meters. The graph shows that, with the exception of the 1st harmonic frequency, all of the harmonics investigated have no effect on the change of amplitude in shaft behavior. This suggests that mass unbalance only influences crack behavior in the 1st harmonic frequency, whereas the remaining harmonics are simply functions of crack effect and are unaffected by mass unbalance. This means that the centrifugal force caused by the mass imbalance will only influence the crack and hence the rotor system, when the shaft rotates at the 1st harmonic frequency. In all other rotations, only the crack effect would influence the shaft. The amplitude of vibration in the first harmonic rotation is greatest at $\beta = 0° = 360°$ and lowest at the angle of symmetry at $\beta = 180°$, while in all other considered harmonics; the vibration amplitudes have constant values.

5 CONCLUSION

A transverse switching crack is modeled to change its position with respect to the direction of mass unbalance. This angle, denoted as β, is incremented by 15° at each step from 0° (when both the crack and unbalance directions are in alignment) to when it comes back to its initial direction, i.e., when reaches 360°. While, orbit plots denote the deflection of the shaft in x and y directions from its ideal geometric axis; FFT plots showed the amplitude of vibrations at different harmonics for different β.

The graphs of β vs x deflection and y deflection bear symmetry from the mid angle of 180°. This happened because the effect on the shaft is the same whether the crack is positioned at the positive radian or negative radian with respect to unbalance direction having the same angle measured from the unbalance axis. While the unbalance tends to open the crack when they are in alignment, i.e., when β is 0° or 360°, it opposes its opening when they are positioned opposite, i.e., when β is 180°. That is, the rotor is weakest when β is 0° or 360° and strongest when β is 180°. Therefore, for reliable operation of rotors in industrial machineries, the centrifugal force must counter the crack opening.

Except for the 1st harmonics, for all β, the vibrations values were constant. The amplitude of vibration of the 1st harmonics varied with respect to β, having its peak value at $\beta = 0° = 360°$ and gradually reducing to its lowest at $\beta = 180°$, symmetrically. Higher amplitude means more inconsistencies in the rotor's performance, while lower amplitude means better stability. This observation confirms that unbalance facilitates crack opening when they lie in the same direction and opposes it when they are placed opposite, as may be noted by industrial and design engineers.

Also, only in 1st harmonics, there exists combined impact of crack and unbalance on the rotor's performance. In other harmonics, the unbalance has no effect, and the rotor's behavior is just a function of crack effect. Furthermore, due to the law of mathematical nature, it was observed that there was no vibration at the 2nd and 4th harmonics.

REFERENCES

[1] N. TEYI, S. SINGH (2022) A decadal review of various modelling and analysis of cracked rotors. *Procedia Structural Integrity* **39** 333-346.

[2] N. TEYI, S. SINGH (2022) A review of application of data science tools in crack identification and localization. *Procedia Structural Integrity* **39** 608-623.

[3] S. WANG, Y. ZI, S. QIAN, B. ZI, C. BI (2018) Effects of unbalance on the nonlinear dynamics of rotors with transverse cracks. *Nonlinear Dynamics* **91** 2755-2772.

[4] J.P. SPAGNOL, H. WU, K. XIAO (2018) Dynamic response of a cracked rotor with an unbalance influenced breathing mechanism. *Journal of Mechanical Science and Technology* **32**(3) 987-1009.

[5] Y. ISHIDA, T. IKEDA, T. YAMAMOTO, N. MASUDA (1988) Vibrations of a rotating shaft containing a transverse crack. *JSME International Journal Series III* **31**(1) 22-29.

[6] K. DARPE, K. GUPTA, A. CHAWLA (2004) Transient response and breathing behaviour of a cracked Jeffcott rotor. *Journal of Sound and Vibration* **272** 207-243.

[7] F. LU, N. ZHANG (2002) Resonance with respect to angular positions of an unbalance of a cracked rotor in a nonlinear rotor system. *International Journal of Acoustics and Vibration* **7**(2) 69-78.

[8] J. GMEZ-MANCILLA, J.J. SINOU, V.R. NOSOV, F. THOUVEREZ, A. ZAMBRANO (2004) The influence of crack-imbalance orientation and orbital evolution for an extended cracked Jeffcott rotor. *C. R. Mecanique* **332** 955-962.

[9] B. MUOZ-ABELLA, L. RUBIO, P. RUBIO (2014) Study of the stress intensity factor of an unbalanced rotating cracked shaft. *Mechanisms and Machine Science* **17** 401-408.

[10] L. RUBIO, B. MUOZ-ABELLA, P. RUBIO, L. MONTERO (2014) Quasistatic numerical study of the breathing mechanism of an elliptical crack in an unbalanced rotating shaft. *Latin American Journal of Solids and Structures* **11** 2333-2350.

[11] L. CHENG , N. LI, X.F. CHEN, Z.J. HE (2011) The influence of crack breathing and imbalance orientation angle on the characteristics of the critical speed of a cracked rotor. *Journal of Sound and Vibration* **330** 2031-2048.

[12] Q. HE, H. PENG, P. ZHAI, Y. ZHEN (2016) The effects of unbalance orientation angle on the stability of the lateral torsion coupling vibration of an accelerated rotor with a transverse breathing crack. *Mechanical Systems and Signal Processing* **75** 330-344.

[13] T.H. PATEL, A.K. DARPE (2005) Influence of crack breathing model on nonlinear dynamics of a cracked rotor. *Journal of Sound and Vibration* **311** 953-972.

[14] Q. HAN, F. CHU (2013) Unbalanced response of cracked rotorbearing system under time-dependent base movements. ASME, International Mechanical Engineering Congress and Exposition. San Diego, USA.

[15] J.R. JAIN, T.K. KUNDRA (2004) Model based online diagnosis of unbalance and transverse fatigue crack in rotor systems. *Mechanics Research Communications* **31** 557-568.

[16] R. GASCH (2008) Dynamic behaviour of the Laval rotor with a transverse crack. *Mechanical Systems and Signal Processing* **22** 790-804.

[17] W. MAYES, W.G.R. DAVIES (1984) Analysis of the response of a multi-rotor- bearing system containing a transverse crack in the rotor. *Journal of Vibration, Acoustics, Stress, and Reliability in Design* **106** 139-145.

[18] R. GASCH (1993) A survey of the dynamic behaviour of a simple rotating shaft with a transverse crack. *Journal of Sound and Vibration* **160**(2) 313-332.

[19] N. TEYI, S. SINGH (2020) Handling Phase Ambiguity in Full Spectrum from FFT. *Lecture Notes in Mechanical Engineering* **810** 519-525.